JPET Fast Forward. Published on May 27, 2016 as DOI: 10.1124/jpet.116.231928
This article has not been copyedited and formatted. The final version may differ from this version.

Title Page

Prediction of altered bile acid disposition due to inhibition of multiple transporters: An integrated approach using sandwich-cultured hepatocytes, mechanistic modeling and simulation

Cen Guo, Kyunghee Yang, Kenneth R. Brouwer, Robert L. St. Claire III and Kim L.R. Brouwer

Division of Pharmacotherapy and Experimental Therapeutics, UNC Eshelman School of Pharmacy, University of North Carolina at Chapel Hill, Chapel Hill, NC (C.G., K.Y., K.L.R.B.); Qualyst Transporter Solutions, Durham, NC (K.R.B., R. S.)

JPET Fast Forward. Published on May 27, 2016 as DOI: 10.1124/jpet.116.231928
This article has not been copyedited and formatted. The final version may differ from this version.

Running Title Page

Running Title: Bile acid disposition predictions in hepatocytes

Address correspondence to:

Kim L.R. Brouwer

UNC Eshelman School of Pharmacy

University of North Carolina at Chapel Hill

CB #7569

Chapel Hill, NC 27599-7569

E-mail address: kbrouwer@email.unc.edu

Telephone: 919 – 962 – 7030

Fax: 919 – 962 – 0644

Number of text pages: 23

Number of tables: 4

Number of figures: 5

Number of references: 49

Number of words in the Abstract: 250

Number of words in the Introduction: 730

Number of words in the Discussion: 1431

Abbreviations: BSEP, bile salt export pump; BSA, Bovine Serum Albumin; CL, clearance; CL_{Bile}, biliary clearance; CL_{BL}, basolateral efflux clearance; CL_{Uptake}, uptake clearance; $CL_{inhibitor}$, clearance in the presence of inhibitor; $C_{t,Cells}$, total concentration in Cells; DDI, drug-drug interaction; d_8-TCA, deuterium-labeled taurocholic acid; f_u, unbound fraction; $f_{u,cell,inhibitor}$, cellular unbound fraction of inhibitor; $f_{u,cyt,inhibitor}$, cytosolic unbound fraction of inhibitor; $f_{u,med}$, unbound fraction in the medium; HBSS, Hanks' balanced salt solution; $[I]_{t,cell}$, cellular total inhibitor concentration; $[I]_{u,cell}$, cellular unbound inhibitor

JPET Fast Forward. Published on May 27, 2016 as DOI: 10.1124/jpet.116.231928
This article has not been copyedited and formatted. The final version may differ from this version.

concentration; $[I]_{t,cyt}$, cytosolic total inhibitor concentration; $[I]_{u,cyt}$, cytosolic unbound inhibitor concentration; $[I]_t$, total inhibitor concentration; $[I]_u$, unbound inhibitor concentration; $[I]_{cell}$, cellular inhibitor concentration; $[I]_{cyt}$, cytosolic inhibitor concentration; $[I]_{u,med}$, medium unbound concentration of inhibitor; MRP, multidrug resistance-associated protein; NTCP, sodium taurocholate co-transporting polypeptide; OATP, organic anion-transporting polypeptide; SCHH, sandwich-cultured human hepatocytes; TCA, taurocholic acid; $X_{t,Cells}$, total amount in Cells; $X_{t,Bile}$, total amount in Bile; $X_{t,Cells+Bile,}$ total amount in Cells+Bile

JPET Fast Forward. Published on May 27, 2016 as DOI: 10.1124/jpet.116.231928
This article has not been copyedited and formatted. The final version may differ from this version.

Abstract

Transporter-mediated alterations in bile acid disposition may have significant toxicological implications. Current methods to predict interactions are limited by the interplay of multiple transporters, absence of protein in the experimental system, and inaccurate estimates of inhibitor concentrations. An integrated approach was developed to predict altered bile acid disposition due to inhibition of multiple transporters using the model bile acid taurocholate (TCA). TCA pharmacokinetic parameters were estimated by mechanistic modeling using sandwich-cultured human hepatocyte data with protein in the medium. Uptake, basolateral efflux, and biliary clearance estimates were 0.63, 0.034, and 0.074 mL/min/g liver, respectively. Cellular total TCA concentrations ($C_{t,Cells}$) were selected as the model output based on sensitivity analysis. Monte Carlo simulations of TCA $C_{t,Cells}$ in the presence of model inhibitors (telmisartan and bosentan) were performed using inhibition constants for TCA transporters and inhibitor concentrations, including cellular total or unbound concentrations ($[I]_{t,cell}$ and $[I]_{u,cell}$), and cytosolic total or unbound concentrations ($[I]_{t,cyt}$ and $[I]_{u,cyt}$). For telmisartan, the model prediction was accurate with an average fold error (AFE) of 0.99-1.0 when $[I]_u$ was used; accuracy dropped when $[I]_t$ was used. For bosentan, AFE was 1.2-1.3 using either $[I]_u$ or $[I]_t$. This difference was evaluated by sensitivity analysis of the cellular unbound fraction of inhibitor ($f_{u,cell,inhibitor}$), which revealed higher sensitivity of $f_{u,cell,inhibitor}$ for predicting TCA $C_{t,Cells}$ when inhibitors exhibited larger ($[I]_{t,cell}/IC_{50}$) values. In conclusion, this study demonstrated the applicability of a framework to predict hepatocellular bile acid concentrations due to drug-mediated inhibition of transporters using mechanistic modeling and cytosolic or cellular unbound concentrations.

Introduction

Transporters play a critical role in the absorption, distribution, and elimination of many drugs and endogenous compounds, such as bile acids. Transporter-mediated drug-bile acid interactions may have significant toxicological implications, such as troglitazone- and bosentan-induced hepatotoxicity due to inhibition of the bile salt export pump (BSEP) (Woodhead JL et al., 2014). Transporter inhibition assays have been adopted by the pharmaceutical industry or included in the recent regulatory guidelines to predict drug-drug interactions (FDA/CDER, 2012). However, the static method, based on the ratio of total plasma maximum concentration (C_{max}) and 50% inhibitory concentration (IC_{50}) or inhibition constant (K_i) of the inhibitor, may not accurately predict the hepatic disposition of victim substrates. Limitations associated with the static method may explain the lack of cholestatic liability of some MRP2 and BSEP inhibitors (Dawson et al., 2012; Pfeifer et al., 2013a). To accurately translate transporter inhibition data (i.e. IC_{50} or K_i) to the prediction of hepatocellular exposure of victim substrates, a number of factors should be considered.

First, hepatic bile acid exposure is regulated by hepatic uptake transporters [e.g. sodium taurocholate co-transporting polypeptide (NTCP) and organic anion-transporting polypeptide (OATP)], as well as canalicular (e.g. BSEP) and basolateral efflux transporters [e.g. multidrug resistance-associated protein 3 (MRP3) and MRP4]. Often, inhibitors of efflux transporters also inhibit uptake transporters, which may exert protective effects (Leslie et al., 2007). However, the static model based on inhibition data from over-expression systems considers uptake and efflux as isolated processes. To overcome this limitation, mechanistic pharmacokinetic modeling coupled with data from sandwich-cultured hepatocytes have been used to deconvolute the relative contribution of various clearance pathways to the disposition of rosuvastatin, mycophenolic acid, and ^{3}H-TCA (Pfeifer et al., 2013c; Matsunaga et al., 2014; Yang et al., 2015). Transporters are expressed and properly localized in the sandwich-cultured hepatocyte system, which can be used to assess the function of multiple transporters (Yang et al., 2016). Thus, this cellular model is uniquely suited to evaluate the interplay of multiple transport pathways and predict the net effect due to inhibition of multiple transporters on the hepatic disposition of victim substrates.

JPET Fast Forward. Published on May 27, 2016 as DOI: 10.1124/jpet.116.231928
This article has not been copyedited and formatted. The final version may differ from this version.

Secondly, the presence of protein in plasma is an important physiological factor. However, albumin at physiological concentrations (e.g., 4% bovine serum albumin; BSA) (Doherty et al., 2006; Wolf et al., 2008) has not been added routinely into *in vitro* experimental systems, such as membrane vesicles, to study transporter-based interactions and assess IC_{50} or K_i values. In addition, according to the "free drug hypothesis", the inhibitory effect is driven by the local unbound concentration of inhibitor, which is the cytosolic unbound inhibitor concentration ($[I]_{u,cyt}$) for efflux transporters, and the medium unbound inhibitor concentration ($[I]_{u,med}$) for uptake transporters (Smith et al., 2010). Some high-throughput methods have been used to measure cellular total and unbound inhibitor concentrations ($[I]_{t,cell}$ and $[I]_{u,cell}$, respectively) (Mateus et al., 2013). However, the isolation of cytosol and measurement of cytosolic total and unbound inhibitor concentrations ($[I]_{t,cyt}$ and $[I]_{u,cyt}$, respectively) adds complexity (Pfeifer et al., 2013b). Thus, $[I]_{t,cyt}$ or $[I]_{u,cyt}$ has not been adopted routinely into the prediction of efflux transporter-based drug interactions. The necessity of measuring the cellular unbound fraction of inhibitor ($f_{u,cell,inhibitor}$) and/or the cytosolic unbound fraction of inhibitor ($f_{u,cyt,inhibitor}$) needs to be assessed.

The purpose of this study was to develop an integrated approach to predict altered bile acid disposition mediated by inhibition of multiple transporters in sandwich-cultured human hepatocytes (SCHH), with a focus on taurocholic acid (TCA), a prototypical bile acid. TCA is generally not metabolized and is commonly used in BSEP and NTCP assays since its transport mechanism is well characterized. First, the hepatobiliary disposition of deuterium-labeled TCA (d_8-TCA) was characterized in the presence of 4% BSA and pharmacokinetic parameters were estimated using mechanistic pharmacokinetic modeling. Total hepatocellular concentrations ($C_{t,Cells}$) were identified as the most sensitive model output according to sensitivity analysis. The effect of model inhibitors, i.e. telmisartan and bosentan, on TCA $C_{t,Cells}$ was predicted based on medium and intracellular inhibitor concentrations (i.e., $[I]_{t,cell}$, $[I]_{u,cell}$, $[I]_{t,cyt}$ and $[I]_{u,cyt}$, separately) and bile acid transporter inhibition data. The predictive performance of the model was evaluated by comparing the simulation results with experimental data and calculating the average fold error (AFE). To determine the necessity of measuring $f_{u,cell,inhibitor}$ for future studies, sensitivity analyses of $f_{u,cell,inhibitor}$ values for the model inhibitors and a set of theoretical inhibitors

were performed. Based on the simulation results, a framework was proposed to help guide future study design.

Materials and Methods

Materials. All chemicals were purchased from Sigma-Aldrich (St. Louis, MO) unless otherwise stated. BioCoat™ cell culture plates and Matrigel® were obtained from BD Biosciences (San Jose, CA). QualGro™ Seeding Medium and QualGro™ Hepatocyte Culture Medium were obtained from Qualyst Transporter Solutions (Durham, NC). d_8-TCA, d_4-TCA (internal standard for d_8-TCA), telmisartan, d_3-telmisartan (internal standard for telmisartan), bosentan, and ambrisentan (internal standard for bosentan) were obtained from Toronto Research Chemicals (ON, Canada). OmniPur® Bovine Serum Albumin (BSA; Fraction V, Heat Shock Isolation) was purchased from Thomas Scientific (Swedesboro, NJ). Pierce BCA Protein Assay was obtained from Thermo Fisher Scientific Inc. (Rockford, IL) and the LDH Cytotoxicity Detection Kit was purchased from Roche Diagnostics (Indianapolis, IN).

Sandwich-Cultured Human Hepatocytes (SCHH). B-CLEAR®-HU Transporter Certified™ cryopreserved human hepatocytes (Lot numbers: HUM4045, HUM4061B, and HUM4059 purchased from Triangle Research Labs, Durham , NC) were seeded in QualGro™ Seeding Medium at a density of 0.4×10^6 cells/well in 24-well BioCoat™ plates and 1.75×10^6 cells/well in 6-well BioCoat™ plates, and cultured in a sandwich configuration (overlaid with Matrigel®) in QualGro™ Hepatocyte Culture Medium as previously reported (Swift et al., 2010). Donors included one Caucasian male, one Caucasian female and one Hispanic female ranging in age from 2 to 44 years old with a body mass index ranging from 18.3 to 30.

Uptake and Efflux Studies of d_8-TCA in SCHH. Uptake and efflux studies of d_8-TCA were performed in SCHH as reported previously with minor modifications (Pfeifer et al., 2013c). Briefly, on day 6 of culture, SCHH seeded in 24-well plates were pre-incubated with standard (Ca^{2+}-containing) or Ca^{2+}-free (Ca^{2+}/Mg^{2+}-free buffer containing EGTA) Hanks' balanced salt solution (HBSS) for 10 min. Incubation with standard HBSS maintains the integrity of the tight junctions, while incubation with Ca^{2+}-free HBSS disrupts the tight junctions, allowing the contents in the bile canaliculi to be washed into the medium (B-CLEAR® technology, Qualyst Transporter Solutions, Durham, NC). Following pre-incubation, the uptake phase was initiated by treating the SCHH with dosing solution (1 μM d_8-TCA in 0.3 mL/well standard

JPET Fast Forward. Published on May 27, 2016 as DOI: 10.1124/jpet.116.231928
This article has not been copyedited and formatted. The final version may differ from this version.

HBSS, with 4% BSA) for up to 20 min. At the end of the uptake phase, the dosing solution was removed, and the SCHH were washed twice with standard or Ca^{2+}-free HBSS at 37°C for 1 min, and incubated with the third application of buffer for a 15-min efflux. Accumulation of d_8-TCA in Cells+Bile (standard HBSS) and Cells (Ca^{2+}-free HBSS) during uptake (2, 5, 10, and 20 min) and efflux (2, 5, 10, and 15 min) phases was determined by terminal sampling of triplicate wells at each time point. During the efflux phase, incubation buffer also was collected at 2, 5, 10, and 15 min. At the end of incubation, the hepatocytes were washed with ice-cold standard HBSS three times and the samples were stored at −80 °C for future analysis.

Determination of Kinetic Parameters for d_8-TCA using Mechanistic Modeling. A model scheme incorporating linear uptake and efflux clearance was adopted (Pfeifer et al., 2013c; Yang et al., 2015) and was fit to d_8-TCA Cells+Bile, Cells, and incubation medium total mass-time data from three individual SCHH experiments (Fig. 1A). The model fitting was performed with Phoenix WinNonlin, v6.3 (Certara, St. Louis, MO) using the stiff estimation method and a power model to account for residual error. Differential Equations 1 to 5 describe the changes in the amount of TCA in the different compartments in this model.

Mass in standard HBSS:

$$\frac{dX^{+}_{t,Buffer}}{dt} = CL_{BL}\times C^{+}_{t,Cells} + K_{Flux}\times X_{t,Bile} - CL_{Uptake}\times C^{+}_{t,Buffer} - K_{Wash}\times X^{+}_{t,Buffer} \quad X^{+}_{Buffer}{}^{\circ} = X_{dose} \qquad (1)$$

Mass in Ca^{2+}-free HBSS:

$$\frac{dX^{-}_{t,Buffer}}{dt} = (CL_{BL} + CL_{Bile})\times C^{-}_{t,Cells} - CL_{Uptake}\times C^{-}_{t,Buffer} - K_{Wash}\times X^{-}_{t,Buffer} \quad X^{-}_{Buffer}{}^{\circ} = X_{dose} \qquad (2)$$

Mass in Cells:

$$\frac{dX^{+or-}_{t,Cells}}{dt} = CL_{Uptake}\times C^{+or-}_{t,Buffer} - (CL_{BL} + CL_{Bile})\times C^{+or-}_{t,Cells} \quad X^{+or-}_{Cell}{}^{\circ} = 0 \qquad (3)$$

Mass in Bile (standard HBSS):

$$\frac{dX_{t,Bile}}{dt} = CL_{Bile}\times C^{+}_{t,Cells} - K_{Flux}\times X_{t,Bile} \quad X_{Bile}{}^{\circ} = 0 \qquad (4)$$

Mass in Cells+Bile (standard HBSS):

JPET Fast Forward. Published on May 27, 2016 as DOI: 10.1124/jpet.116.231928
This article has not been copyedited and formatted. The final version may differ from this version.

$$\frac{dX_{t,Cells+Bile}}{dt} = \frac{dX_{t,Bile}}{dt} + \frac{dX^{+}_{t,Cells}}{dt} \qquad X^{\circ}_{Cells+Bile} = 0 \qquad (5)$$

where $C_{t,Cells}$ represents the total intracellular concentration, and was calculated as X_{Cells}/V_{Cells}; V_{Cells} was calculated and fixed using the protein content of each preparation and a value of 7.4 μL/mg protein (Pfeifer et al., 2013c; Yang et al., 2015); "+" and "-" refer to Ca^{2+}-containing (standard HBSS) and Ca^{2+}-free HBSS, respectively; $X_{t,Cells}$ represents the total amount in Cells; $X_{t,Cells+Bile}$ represents the total amount in Cells+Bile; $X_{t,Bile}$ represents the total amount in Bile; $C_{t,Buffer}$ represents the total Buffer concentration; V_{Buffer} was set as a constant (0.3 mL); CL_{Uptake} represents total uptake clearance; CL_{BL} represents total basolateral efflux clearance; CL_{Bile} represents total biliary clearance; and K_{Flux} represents the first-order rate constant that describes the flux from bile networks into the medium due to periodic contraction of the bile canalicular networks (Pfeifer et al., 2013c)(Oshio and Phillips, 1981; Phillips et al., 1982; Lee et al., 2010). Clearance units (μL/min/mg protein) were converted to mL/min/g liver based on the protein content in liver tissue (90 mg protein/g liver) (Sohlenius-Sternbeck, 2006). To represent the 1-min wash step, K_{wash} was activated for 1min at the end of the 20-min uptake phase using an if-then statement. K_{wash} was fixed at $1x10^{4}$ min^{-1}, which was sufficient to eliminate the d_8-TCA from the buffer compartment based on simulations. Initial parameter estimates were obtained from previous reports for ^{3}H-TCA (Yang et al., 2015).

Sensitivity Analyses of Model Output. Sensitivity analyses were conducted using Berkeley-Madonna v.8.3.11 to identify the most sensitive SCHH model output with respect to changes in clearance (CL). Different model outputs measured in the SCHH experiment, including the total concentration of TCA in Cells ($C_{t,Cells}$), total amount in Cells+Bile ($X_{t,Cells+Bile}$), total amount in Bile ($X_{t,Bile}$), ratio of the total amount of TCA in Cells to the total amount of TCA in Cells+Bile ($X_{t,Cells}/X_{t,Cells+Bile}$), ratio of the total amount of TCA in Bile to the total amount of TCA in Cells ($X_{t,Bile}/X_{t,Cells}$), and ratio of the total amount in Bile to the total amount in Cells+Bile ($X_{t,Bile}/X_{t,Cells+Bile}$), were simulated throughout the time course assuming CL_{Uptake} and CL_{Efflux} were inhibited by 0- to 0.99-fold. CL_{Efflux} was defined as $CL_{Bile}+CL_{BL}$, assuming CL_{Bile} and CL_{BL} were impaired to the same extent. The simulated fold-changes of the model

JPET Fast Forward. Published on May 27, 2016 as DOI: 10.1124/jpet.116.231928
This article has not been copyedited and formatted. The final version may differ from this version.

output values at steady state (120 min) were plotted against the fraction of inhibition of CL_{Uptake} and CL_{Efflux} in a 3-D fashion using SigmaPlot v.11 (San Jose, California). The fraction of inhibition was calculated as $(CL-CL_{inhibitor})/CL$, where CL and $CL_{inhibitor}$ represent the clearance in the absence and presence of inhibitor, respectively. A higher fraction of inhibition means more potent inhibition.

Determination of Cellular and Cytosolic Total and Unbound Concentrations of Inhibitors ($[I]_{t,cell}$, $[I]_{t,cyt}$, $[I]_{u,cell}$, and $[I]_{u,cyt}$, respectively). SCHH seeded in 6-well plates were pre-incubated with Ca^{2+}-free HBSS for 10 min, followed by a 20-min incubation with dosing solution of model inhibitors (1 and 10 μM of telmisartan, or 0.8 and 8 μM of bosentan in standard HBSS with 4% BSA). After the incubation, cells were washed with ice-cold HBSS three times and stored at −80°C for future analysis. All the incubations in this study were performed at 37°C.

Cells were fractionated as reported previously with minor modification (Pfeifer et al., 2013b). Briefly, hepatocytes from the same treatment group were pooled and homogenized by passing the cells in fractionation buffer through a 27g needle 20 times to disrupt the cell membranes. The resultant cell lysate was subject to 10,000g centrifugation for 10 min at 4°C to isolate cytosol (supernatant) from other cell debris. The protein content of cell lysate was determined by Pierce BCA Protein Assay. The LDH activity of each fraction (i.e. cell lysate, cytosol and suspended pellet) was measured using an LDH cytotoxicity detection kit to reflect LDH recovery from cytosol. Glucose-6-phosphatase, succinate dehydrogenase, and acid phosphatase activity of each fraction were measured to assess microsomal, mitochondrial, and lysosomal contamination, respectively. The percentage of the organelle-specific enzyme activity measured in each fraction was calculated in comparison to the whole lysate to assess recovery. The unbound fraction (f_u) was determined by equilibrium dialysis as previously reported (Pfeifer et al., 2013b). Briefly, triplicate aliquots of samples (dosing solution, cell lysate and cytosol) were loaded into a 96-well equilibrium dialysis apparatus (HTDialysis, LLC; Gales Ferry, CT) and incubated at 37°C for 8 hours with shaking, which was sufficient to achieve equilibrium for most compounds (Banker et al., 2003). The f_u was back-calculated based on Equation 6 to account for dilution during the homogenization and fractionation process as described previously (Kalvass et al., 2007).

JPET Fast Forward. Published on May 27, 2016 as DOI: 10.1124/jpet.116.231928
This article has not been copyedited and formatted. The final version may differ from this version.

$$\text{Undiluted } f_u = \frac{1/D}{\left(\left(\frac{1}{fu_{measured}}\right)-1\right)+1/D} \qquad (6)$$

where D represents the dilution factor.

The total mass of inhibitors in cell lysate and cytosol samples was measured. Cellular concentrations were calculated by dividing the mass by the estimated cellular volume of 7.4 μL/mg protein (Pfeifer et al., 2013c; Yang et al., 2015); cytosolic concentrations were calculated by dividing the mass by the estimated cytosolic volume, assuming cytosolic volume represents 70% of cellular volume (Grunberg et al., 2009). Unbound inhibitor concentrations ($[I]_u$) were calculated as the product of total inhibitor concentration ($[I]_t$) and f_u.

Simulation of Inhibitor Effects on TCA Disposition and Comparison with Experimental Results. d_8-TCA $C_{t,Cells}$ were measured after the following treatments: a 10-min pre-incubation of SCHH with telmisartan (1 or 10 μM) or bosentan (0.8 or 8 μM) in Ca^{2+}-free HBSS with 4% BSA, followed by a 10-min co-incubation with d_8-TCA (1 μM) and telmisartan or bosentan in standard HBSS with 4% BSA. TCA $C_{t,Cells}$ after 10-min uptake were simulated using Equations 1-5 and $CL_{inhibitor}$ values, which were calculated using Equations 7-10.

$$CL_{Uptake,inhibitor} = 0.7 \times CL_{Uptake}/\left(1 + \frac{[I]_{u,med}}{IC_{50,NTCP}}\right) + 0.3 \times CL_{Uptake}/\left(1 + \frac{[I]_{u,med}}{IC_{50,OATP1B1}}\right) \qquad (7)$$

$$CL_{BL,inhibitor} = CL_{BL}/\left(1 + \frac{[I]_{cell}}{IC_{50,MRP3}}\right) \qquad (8)$$

$$CL_{BL,inhibitor} = CL_{BL}/\left(1 + \frac{[I]_{cell}}{IC_{50,MRP4}}\right) \qquad (9)$$

$$CL_{Bile,inhibitor} = CL_{Bile}/\left(1 + \frac{[I]_{cell}}{IC_{50,BSEP}}\right) \qquad (10)$$

where $CL_{Uptake,Inhibitor}$, $CL_{BL,Inhibitor}$, and $CL_{Bile,Inhibitor}$ represent the CL_{Uptake}, CL_{BL}, and CL_{Bile} of TCA in the presence of inhibitors, respectively; $[I]_{u,med}$ represents the unbound concentration of inhibitor in the medium; $[I]_{cell}$ represents the cellular inhibitor concentration, and different fractions of cellular concentration were used in the simulation, including $[I]_{t,cell}$, $[I]_{u,cell}$, $[I]_{t,cyt}$, $[I]_{u,cyt}$ (obtained as described in the previous section; values are shown in Table 3). The mean IC_{50} values for each transporter in Table 1

JPET Fast Forward. Published on May 27, 2016 as DOI: 10.1124/jpet.116.231928
This article has not been copyedited and formatted. The final version may differ from this version.

were used with the assumptions that NTCP and OATPs contribute 70% and 30%, respectively, to CL_{Uptake} (Shitara et al., 2003; De Bruyn et al., 2014), BSEP mediates CL_{Bile} (Noe et al., 2002; Chandra and Brouwer, 2004; Hayashi et al., 2005), and CL_{BL} is governed by MRP3 (Zhang et al., 2003) or MRP4 (Rius et al., 2006). Since the relative contribution of MRP3 and MRP4 is unknown, two extremes were simulated assuming MRP3 (Equation 8) or MRP4 (Equation 9) contributes 100% to CL_{BL}. Monte Carlo simulations of 40 individuals were performed 10 times using parameter estimates and the associated variance (Table 2); clearance was assumed to be normally distributed. The fold changes in the TCA $C_{t,Cells}$ in the presence vs. the absence of inhibitors were calculated and compared between predicted and observed results. Arithmetic mean and 95% confidence intervals of the fold changes were reported. The precision of the prediction was evaluated using the average fold error (AFE) (Equation 11)(Vildhede et al., 2016).

$$AFE=10^{\frac{\sum\log\left(\frac{Predited\ fold\ change}{Observed\ fold\ change}\right)}{Number\ of\ predictions}} \quad (11)$$

Sensitivity Analyses of Model Input. The sensitivity of $f_{u,cell,inhibitor}$, a compound-specific parameter for telmisartan and bosentan, on model output (TCA $C_{t,Cells}$) was evaluated. Monte Carlo simulations were performed to predict the fold changes in the TCA $C_{t,Cells}$ at steady state (120 min) using parameters and the associated variance in Table 2, and Equations 1-5 and 7, 8, 10, where $[I]_{cell}=[I]_{t,cell}\times f_{u,cell,inhibitor}$. Different $f_{u,cell,inhibitor}$ values (0.02-1) were used in the simulations. $[I]_{t,cell}$ and $[I]_{u,med}$ from SCHH incubated with telmisartan (1 or 10 μM) and bosentan (0.8 or 8 μM) were obtained from Table 3, as described above.

Furthermore, to generalize the sensitivity analysis of $f_{u,cell,inhibitor}$ to a broader range of inhibitors, TCA $C_{t,Cells}$ at steady state (120 min) in the presence of theoretical inhibitors with different ($[I]_{t,cell}/IC_{50}$) values (ranging from 0.5 to 60) were simulated assuming $f_{u,cell,inhibitor}$=1 or 0.02, respectively. In these simulations, IC_{50} represented the inhibitory potency against efflux transporters, and CL_{BL} and CL_{Bile} were assumed to be inhibited to the same extent. All simulations were performed with and without 50% inhibition of CL_{Uptake}.

LC-MS/MS Analysis. Lysis solution [500 µL of 70% methanol/30% water containing internal standard (25 nM d_4-TCA, d_3-telmisartan, or ambrisentan)] was added to each well of previously frozen 24-well or 6-well plates containing study samples. Plates were shaken for ~15 min and the cell lysate solution was filtered, evaporated to dryness and reconstituted. Medium samples were extracted with 300 µL of 100% methanol containing internal standard, filtered, evaporated, and reconstituted. Standards and quality control samples were prepared by adding a known amount of standards into a blank cell plate or medium followed by the same sample processing methods with test samples. d_8-TCA samples were reconstituted in 60% methanol/40% water containing 10 mM ammonium acetate and analysed by LC-MS/MS using a Shimadzu binary HPLC system (Columbia, MD) and Thermo Electron TSQ® Quantum Discovery MAX ™ (Waltham, MA) with an Ion Max ESI source using negative electrospray ionization mode. Samples (10 µL) were injected onto a 100×1.0 mm Hypersil Gold™ C_{18} column (Thermo Scientific, Bellefonte, PA). The mobile phase was methanol/water with 0.5 mM ammonium acetate at a flow rate of 50 µL/min. The transitions monitored (parent m/z > product m/z) were 522 > 128 and 518 > 124 for d_8-TCA and d_4-TCA. The calibration curve range was 0.5-100 pmol/well. Telmisartan samples were reconstituted in 70% methanol/30% water with 0.1% formic acid and analysed by the same LC-MS/MS system using positive electrospray ionization mode. The mobile phase was methanol/water with 0.1% formic acid at a flow rate of 50 µL/min. The transitions monitored were 515.2 > 276.2 and 518.2 > 279.2 for telmisartan and d_3-telmisartan, respectively. The calibration curve range was 0.01-10 pmol/well. Bosentan samples were reconstituted in 60% methanol/30% water with 0.1% formic acid and analysed by LC-MS/MS using a Shimadzu binary HPLC system (Columbia, MD) and Applied Biosystems API-3000 mass spectrometer operated in positive electrospray ionization mode. Samples (10 µL) were loaded onto a 100×1.0 mm Hypersil Gold™ C_{18} column (Thermo Scientific, Bellefonte, PA). The mobile phase was acetonitrile/water with 0.2% formic acid. The transitions monitored were 522.3 > 202.2 for bosentan and 379.1 > 303.1 for ambrisentan. The calibration curve range was 0.05-50 pmol/well. Acceptance criteria for % accuracy of back calculated values was 15-20%. TCA accumulation in cell lysate was corrected for nonspecific binding to the BioCoat™ plate without cells.

JPET Fast Forward. Published on May 27, 2016 as DOI: 10.1124/jpet.116.231928
This article has not been copyedited and formatted. The final version may differ from this version.

Results:

Hepatobiliary Disposition of d_8-TCA in SCHH

The model scheme depicted in Fig 1A, and Equations 1-5, were used to describe SCHH data (TCA in Cells+Bile, Cells, and incubation medium) from three human livers. Data were analyzed as three independent data sets and were well described by the mechanistic model (individual fits are not shown). The mean (±S.E.M.) data and simulated mass-time profiles generated using the mean of best-fit parameter estimates from the three SCHH data sets (Table 2) are presented in Fig. 1B. After 20-min uptake, TCA $C_{t,Cells}$ was 5.6 μM. The mean kinetic parameters and the associated variance estimated by fitting the differential Equations 1-5 to TCA mass-time data from three independent SCHH preparations are presented in Table 2. The estimated total CL_{Uptake} of TCA was approximately one order of magnitude greater than total CL_{Bile} and total CL_{BL} estimates; TCA CL_{Bile} was approximately 2-fold greater than CL_{BL}. These parameter estimates were used in the following simulations.

Sensitivity Analyses of Model Output

To identify a model output that was sensitive to impairment in both CL_{Uptake} and CL_{Efflux}, the simulated fold changes in different endpoints of the SCHH assay (at steady state) were plotted against the fraction of inhibition of CL_{Uptake} and CL_{Efflux} in Fig. 2, where $CL_{Efflux} = CL_{BL}+CL_{Bile}$. The most sensitive model output to both CL_{Uptake} and CL_{Efflux} of TCA was $C_{t,Cells}$. $C_{t,Cells}$ decreased to 0.01-fold of baseline when CL_{Uptake} was inhibited by 99% and CL_{Efflux} was not inhibited, and increased to approximately15-fold of baseline when CL_{Efflux} was inhibited by 99% and CL_{Uptake} was not inhibited. Other endpoints were only sensitive to either CL_{Uptake} (e.g., $X_{t,Cells+Bile}$) or CL_{Efflux} (e.g., $X_{t,Bile}$, $X_{t,Bile}/X_{t,Cells}$ and $X_{t,Bile}/X_{t,Cells+Bile}$) and the fold changes were less pronounced. Therefore, the TCA $C_{t,Cells}$ was chosen as the model output in the following simulations to reflect the altered hepatobiliary disposition of TCA in the presence of inhibitors.

Determination of Cellular and Cytosolic Total and Unbound Concentrations of Inhibitors

After 20-min incubation with SCHH, the total and unbound concentrations of telmisartan and bosentan in medium, whole cell lysates, and cytosol were measured; the results are reported in Table 3. The cytosol was isolated with ~100% recovery (based on the LDH assay; data not shown) and low contamination of

JPET Fast Forward. Published on May 27, 2016 as DOI: 10.1124/jpet.116.231928
This article has not been copyedited and formatted. The final version may differ from this version.

subcellular organelles (3% recovery of the enzyme marker for microsomal contamination; 5% recovery of the enzyme marker for mitochondrial contamination). As shown in Table 3, telmisartan was highly bound in the whole cell lysate and cytosol ($f_{u,cell,inhibitor}$=0.09-0.13 and $f_{u,cyt,inhibitor}$=0.05-0.08); the cytosolic unbound telmisartan concentrations were only 5.3-8% of the total concentrations in the cell. The unbound fraction of bosentan was higher than telmisartan ($f_{u,cell,inhibitor}$=0.22-0.41 and $f_{u,cyt,inhibitor}$=0.12); the cytosolic unbound bosentan concentration was 12% of the total concentration in the whole cell. More than one-half of the amount of telmisartan (62%-70%) and bosentan (58%-63%) in the whole cell lysate was recovered in the cytosol. Considering that cytosolic volume represents ~70% of the cellular volume (Grunberg et al., 2009), the cytosolic and cellular total concentrations were similar.

Comparison of Simulated and Observed TCA Disposition in the Presence of Inhibitors

The fold changes in the TCA $C_{t,Cells}$ in the presence of inhibitors (telmisartan and bosentan) vs. in the absence of inhibitors were simulated and compared to experimental results (Table 4). Monte Carlo simulations were performed for 40 individuals and repeated 10 times using either Equation 8 or Equation 9 assuming either MRP3 or MRP4 mediated the basolateral efflux of TCA. The simulation results were similar and therefore, only the simulations based on MRP3 inhibition were presented, since MRP3 expression was reported to be higher than MRP4 in human liver and hepatocytes (Vildhede et al., 2015; Wisniewski et al., 2016). In the prediction of telmisartan's effect on TCA $C_{t,Cells}$, the AFE of simulations using $[I]_{u,cell}$ and $[I]_{u,cyt}$ was 1.0 and 0.99, respectively. The 95% confidence interval of the simulation results overlapped with the range of observed data. When $[I]_{t,cell}$ and $[I]_{t,cyt}$ were used in the simulation, TCA $C_{t,Cells}$ was over-predicted and the AFE was 1.4 and 1.3, respectively. In the prediction of bosentan's effect, the mechanistic model slightly over-predicted the fold change for TCA $C_{t,Cells}$, with an average fold error of 1.2-1.3, no matter which inhibitor concentration was used. According to the simulations (Supplementary Figure 1), telmisartan-induced changes in TCA $C_{t,Cells}$ increased as the uptake phase was extended. After a 30-min uptake phase, the simulated TCA $C_{t,Cells}$ for telemisartan based on $[I]_{t,cell}$ was 3-fold of the simulation based on $[I]_{u,cyt}$.

JPET Fast Forward. Published on May 27, 2016 as DOI: 10.1124/jpet.116.231928
This article has not been copyedited and formatted. The final version may differ from this version.

Sensitivity Analyses of Model Inputs

Since the use of $[I]_u$ or $[I]_t$ affected the simulation of TCA $C_{t,Cells}$ differently for telmisartan and bosentan, sensitivity analysis of $f_{u,cell,inhibitor}$ for telmisartan and bosentan was performed by simulating TCA $C_{t,Cells}$ using $[I]_{t,cell}$ of telmisartan and bosentan and various $f_{u,cell,inhibitor}$ values (0.02-1) (Table 3). Simulated TCA $C_{t,Cells}$ at steady state were expressed as the mean and standard deviation of fold changes over baseline (without inhibitors) (shown in Fig. 3). The TCA $C_{t,Cells}$ was sensitive to changes in $f_{u,cell,inhibitor}$ for telmisartan but not for bosentan at both the low and high dosing concentrations. At the low dosing concentration, the mean fold change in the TCA $C_{t,Cells}$ increased from 0.8 to 2.5 when the $f_{u,cell,inhibitor}$ for telmisartan changed from 0.02 to 1; the mean fold change in the TCA $C_{t,Cells}$ increased from 0.8 to 1 when the $f_{u,cell,inhibitor}$ for bosentan changed from 0.02 to 1. At the high dosing concentration, the mean fold change ranged from 0.9 to 4 when the $f_{u,cell,inhibitor}$ for telmisartan changed from 0.02 to 1; the mean fold change ranged from 0.8 to 1.5 when the $f_{u,cell,inhibitor}$ for bosentan changed from 0.02 to 1. (Fig. 3).

To explore the differential sensitivity of TCA $C_{t,Cells}$ to $f_{u,cell,inhibitor}$ for different inhibitors, the TCA $C_{t,Cells}$ in the presence of a set of theoretical inhibitors with various ($[I]_{t,cell}/IC_{50}$) values were simulated using $f_{u,cell,inhibitor}$=1 and 0.02 (Fig. 4). For inhibitors with the same ($[I]_{t,cell}/IC_{50}$) value, if the inhibitor exhibited no intracellular binding (i.e., $f_{u,cell,inhibitor}$=1), the simulated fold change in the TCA $C_{t,Cells}$ was greater than when the inhibitor exhibited extensive intracellular binding (i.e., $f_{u,cell,inhibitor}$=0.02). As the ($[I]_{t,cell}/IC_{50}$) value increased, the difference in simulated TCA $C_{t,Cells}$ between $f_{u,cell,inhibitor}$ =1 and 0.02 increased. For inhibitors with ($[I]_{t,cell}/IC_{50}$) >1, the predicted TCA $C_{t,Cells}$ when $f_{u,cell,inhibitor}$ =1 was more than twice of the predicted TCA $C_{t,Cells}$ when $f_{u,cell,inhibitor}$ =0.02. These relationships were the same with or without 50% inhibition of CL_{Uptake} (data not shown).

JPET Fast Forward. Published on May 27, 2016 as DOI: 10.1124/jpet.116.231928
This article has not been copyedited and formatted. The final version may differ from this version.

Discussion

In this study, an integrated approach was developed to predict the net effect of inhibition of multiple transporters on the hepatocellular disposition of the model bile acid TCA based on inhibition constants and SCHH data using mechanistic modeling. Importantly, the intracellular binding of inhibitors was considered in the simulations, and a strategy was proposed to determine whether it is necessary to measure the intracellular binding *a priori*.

The following assumptions were made for the mechanistic modeling. Linear kinetics was assumed because the unbound concentration of TCA in the medium ($f_{u,med}$×1 µM, where $f_{u,med}$ refers to the unbound fraction of TCA in the medium equivalent to 0.15 in 4% BSA)(Wolf et al., 2008) was below the K_m of TCA for the uptake transporter NTCP (5-20 µM) and OATPs (5.8-71.8 µM) (Shitara et al., 2003; Nozawa et al., 2004; Mita et al., 2006; De Bruyn et al., 2014). In addition, the cellular total concentration of TCA (5.6 µM) after 20-min uptake was below the K_m for the efflux transporters BSEP (6.2 µM) (Hayashi et al., 2005), MRP3 (30 µM) and MRP4 (7.7 µM); if intracellular binding is taken into account, the cellular unbound concentration of TCA would be even lower. Passive diffusion was not included in the model because active uptake plays a major role in the hepatocellular accumulation of TCA (Shitara et al., 2003; Mita et al., 2006).

To simulate the effects of inhibitors on TCA disposition, Equations 7-10 were used. Due to low TCA concentrations, Equations 7-10 held true regardless of the mechanisms of inhibition and the IC_{50} value was substituted for K_i. The inhibitory effects of metabolites of telmisartan and bosentan were assumed to be negligible. There are no literature reports about inhibitory effects of telmisartan metabolites on human bile acid transporters. Although a bosentan metabolite, Ro 47-8634, was reported to be an inhibitor of rat Bsep (K_i=8.5 µM) (Fattinger et al., 2001), the intracellular concentration of this metabolite in human SCHH is less than 5% of bosentan (Matsunaga et al., 2015). In addition, the concentration of this metabolite in human plasma (Dingemanse et al., 2002) and feces (Weber et al., 1999) is much lower than bosentan. Both MRP3 and MRP4 have been reported to contribute to the basolateral efflux of TCA without consensus on the relative contribution. The expression of MRP3 is higher than

JPET Fast Forward. Published on May 27, 2016 as DOI: 10.1124/jpet.116.231928
This article has not been copyedited and formatted. The final version may differ from this version.

MRP4 in human liver and hepatocytes; while the affinity of TCA towards MRP4 (K_m=7.7 μM) (Rius et al., 2006) is higher than MRP3 (K_m=30 μM) (Zhang et al., 2003). Akita and colleagues reported that TCA was not transported to a significant degree by MRP3 (Akita et al., 2002). Therefore, two extreme scenarios were simulated assuming 100% contribution of either MRP3 or MRP4; the simulation results were similar so MRP3 was selected as the main basolateral efflux transporter for subsequent simulations.

In the current study, a physiologic concentration of protein (4% BSA) was added to mimic the *in vivo* scenario. Using the mechanistic model, the estimated total CL_{Uptake} of TCA was 0.63 mL/min/g liver (Table 2) and the unbound CL_{Uptake} of TCA was 4.2 mL/min/g liver (calculated as total $CL_{Uptake}/f_{u,med}$). This value is close to the reported unbound CL_{Uptake} (2.2 mL/min/g liver) (Yang et al., 2015). CL_{BL} and CL_{Bile} were similar to values reported previously (CL_{BL}=0.042 mL/min/g liver and CL_{Bile}=0.14 mL/min/g liver) (Yang et al., 2015).

In this study, we leveraged SCHH and a mechanistic model to evaluate the net effect of uptake and efflux. The comparison between simulated and experimental results for telmisartan and bosentan provided an example of the applicability of this approach to predict the net effect of inhibition at multiple sites on the disposition of a model bile acid (Table 4). This applicability is important because the interplay of multiple transporters is common. Examples of dual inhibitors of BSEP and NTCP include the non-hepatotoxic drugs pioglitazone, telmisartan, and reserpine (Morgan et al., 2010; Dong et al., 2014) as well as the hepatotoxic compound troglitazone (Yang et al., 2014) (Morgan et al., 2010). Some compounds are dual inhibitors of both basolateral uptake and efflux of TCA, such as alpha-naphthylisothiocyanate (Guo et al., 2014).

The slight differences between model predicted and experimental results observed for bosentan's effect on TCA $C_{t,Cells}$ could be attributed to the model assumptions discussed earlier. It should be noted that inhibitor-mediated alterations in TCA $C_{t,Cells}$ was not extensive due to the short 10-min uptake phase in this study and simultaneous inhibition of uptake and efflux. A more pronounced alteration in TCA $C_{t,Cells}$ could be achieved by extending the uptake phase (Supplementary Figure 1). However, accurate measurement of the TCA $C_{t,Cells}$ after an uptake phase >30 min is technically challenging in sandwich-

JPET Fast Forward. Published on May 27, 2016 as DOI: 10.1124/jpet.116.231928
This article has not been copyedited and formatted. The final version may differ from this version.

cultured hepatocytes. When Ca^{2+} is present during an extended uptake phase, the tight junctions reseal yielding a measured $X_{t,Cells+Bile}$ instead of $X_{t,Cells}$ (Pfeifer et al., 2013c).

This is the first study to evaluate the impact of using different cellular inhibitor concentrations to predict transporter-mediated interactions in SCHH. Use of cytosolic concentrations marginally improved the prediction of telmisartan's effects; the AFE dropped by ≤ 0.1 when $[I]_{cyt}$ instead of $[I]_{cell}$ was used. This difference was minor because telmisartan was recovered primarily in the cytosol (62-70% of the total mass) and the cytosolic concentration approximated the cellular concentration. The impact of using $[I]_{cyt}$ instead of $[I]_{cell}$ would likely be greater for drugs that are trapped in subcellular organelles, such as furamidine (Pfeifer et al., 2013b). Different enzymatic markers were used to evaluate the purity and recovery of cytosol. However, membrane-anchored proteins (e.g., the endoplasmic reticulum marker glucose-6-phosphatase) would not be able to detect whether content in the endoplasmic reticulum lumen had been released into the cytosol. Lumen protein markers [e.g., ERp57 (Coe et al., 2010) or Glucosidase II (Zuber et al., 2000)] could be measured in future studies to exclude this possibility.

In drug-drug interaction (DDI) evaluations, $[I]_{t,cell}$ is used commonly to avoid false-negative predictions by assessing the "worst-case scenario", but this value can lead to false-positive predictions. Pfeifer et al. reported that using $[I]_{u,cell}$ of ritonavir correctly predicted no clinical MRP2-mediated DDI between ritonavir and ^{99m}Tc-mebrofenin, while predictions based on $[I]_{t,cell}$ of ritonavir led to a false positive prediction of DDI liability (Pfeifer et al., 2013a). In the case of telmisartan, simulations using $[I]_{t,cell}$ and $[I]_{t,cyt}$ slightly overpredicted TCA $C_{t,Cells}$ compared to simulations using $[I]_{u,cell}$ and $[I]_{u,cyt}$. Unlike telmisartan, simulations for bosentan's effect on TCA $C_{t,Cells}$ were similar regardless of whether total or unbound, cellular or cytosol, concentrations of bosentan were employed (Table 4). Sensitivity analysis revealed the differential sensitivity of TCA $C_{t,Cells}$ to $f_{u,cell,inhibitor}$ for telmisartan and bosentan (Fig. 3). This difference suggested that although it is ideal to use $[I]_u$, it is not necessary to measure $f_{u,cell,inhibitor}$ and use $[I]_{u,cell}$ for every inhibitor. Simulations of a set of theoretical inhibitors showed that inhibitors with high ($[I]_{t,cell}/IC_{50}$) values were more sensitive to changes in $f_{u,cell,inhibitor}$ (Fig. 4). For example, when ($[I]_{t,cell}/IC_{50}$) was >1, the simulation assuming no protein binding over-predicted TCA $C_{t,Cells}$ by twice or

JPET Fast Forward. Published on May 27, 2016 as DOI: 10.1124/jpet.116.231928
This article has not been copyedited and formatted. The final version may differ from this version.

more. Inhibitors with large ($[I]_{t,cell}/IC_{50}$) values either tend to accumulate in the cells or serve as strong inhibitors of efflux transporters. In these cases, ignoring protein binding would greatly impact the prediction, and thus, $f_{u,cell,inhibitor}$ needs to be measured. The ($[I]_{t,cell}/IC_{50}$) value of telmisartan was 3.6 at the 10 μM dose level and the ($[I]_{t,cell}/IC_{50}$) value of bosentan was 0.8 at the 8 μM dose level. This difference could explain the greater sensitivity of predicted TCA $C_{t,Cells}$ to changes in $f_{u,cell,inhibitor}$ of telmisartan compared to bosentan.

Based on the results of these studies, a framework was proposed to predict the net effect of drug-bile acid interactions mediated by inhibition of multiple transporters (Fig. 5). The kinetic parameters (CL_{Uptake}, CL_{Bile}, and CL_{BL}) of the victim bile acid (e.g. TCA) are estimated by mechanistic modeling; in the presence of inhibitors, the clearance values are affected by $[I]_{u,med}$ or $[I]_{cell}$ and IC_{50} or K_i values. The choice of which $[I]_{cell}$ value to use (e.g., $[I]_{t,cell}$, $[I]_{t,cyt}$, $[I]_{u,cell}$, $[I]_{u,cyt}$) depends on the sensitivity of the model output to $f_{u,cell,inhibitor}$, which is determined by the ($[I]_{t,cell}/IC_{50}$) value of the inhibitor. If this value is high, the model output, $C_{t,Cells}$, is sensitive to changes in $f_{u,cell,inhibitor}$. In these cases, it is critical to measure $f_{u,cell,inhibitor}$, as demonstrated in this study. For inhibitors that sequester in subcellular organelles, it may be necessary to isolate cytosol and measure $[I]_{u,cyt}$. Finally, the altered hepatocellular disposition of the victim bile acid, namely $C_{t,Cells}$, can be simulated using $CL_{inhibitor}$ (calculated using Equations 7-10). This approach could be applied to evaluate transporter-mediated interactions involving other victim substrates (e.g. hepatotoxic bile acids), which would have significant toxicological implications.

Acknowledgements

Phoenix software was generously provided to the Division of Pharmacotherapy and Experimental Therapeutics, UNC Eshelman School of Pharmacy, by Certara as a member of the Pharsight Academic Center of Excellence Program.

We thank Dr. Weslyn Friley for her analytical support.

Authorship Contributions

Participated in research design: Guo, Yang, Brouwer, K.R., Brouwer, K.L.R.

Conducted experiments: Guo, St. Claire

Performed data analysis: Guo, Yang, Brouwer, K.R., Brouwer, K.L.R.

Wrote or contributed to the writing of the manuscript: Guo, Yang, Brouwer, K.L.R.

References

Akita H, Suzuki H, Hirohashi T, Takikawa H and Sugiyama Y (2002) Transport activity of human MRP3 expressed in Sf9 cells: comparative studies with rat MRP3. *Pharm Res* **19**:34-41.

Ansede JH, Smith WR, Perry CH, St Claire RL, 3rd and Brouwer KR (2010) An in vitro assay to assess transporter-based cholestatic hepatotoxicity using sandwich-cultured rat hepatocytes. *Drug Metab Dispos* **38**:276-280.

Banker MJ, Clark TH and Williams JA (2003) Development and validation of a 96-well equilibrium dialysis apparatus for measuring plasma protein binding. *J pharm Sci* **92**:967-974.

Chandra P and Brouwer KLR (2004) The complexities of hepatic drug transport: current knowledge and emerging concepts. *Pharml Res* **21**:719-735.

Coe H, Jung J, Groenendyk J, Prins D and Michalak M (2010) ERp57 modulates STAT3 signaling from the lumen of the endoplasmic reticulum. *J Biol Chem* **285**:6725-6738.

Dawson S, Stahl S, Paul N, Barber J and Kenna JG (2012) In vitro inhibition of the bile salt export pump correlates with risk of cholestatic drug-induced liver injury in humans. *Drug Metab Dispos* **40**:130-138.

De Bruyn T, Sempels W, Snoeys J, Holmstock N, Chatterjee S, Stieger B, Augustijns P, Hofkens J, Mizuno H and Annaert P (2014) Confocal imaging with a fluorescent bile acid analogue closely mimicking hepatic taurocholate disposition. *J pharm sci* **103**:1872-1881.

Doherty MM, Poon K, Tsang C and Pang KS (2006) Transport is not rate-limiting in morphine glucuronidation in the single-pass perfused rat liver preparation. *J Pharmacol Exp Ther* **317**:890-900.

Dong Z, Ekins S and Polli JE (2014) Quantitative NTCP pharmacophore and lack of association between DILI and NTCP Inhibition. *Eur J Pharm Sci* **66c**:1-9.

Fattinger K, Funk C, Pantze M, Weber C, Reichen J, Stieger B and Meier PJ (2001) The endothelin antagonist bosentan inhibits the canalicular bile salt export pump: a potential mechanism for hepatic adverse reactions. *Clin Pharmacol Ther* **69**:223-231.

FDA/CDER US (2012) Drug interaction studies - study design, data analysis, and implications for dosing and labeling recommendations, DRAFT GUIDANCE.

Grunberg W, Staufenbiel R, Constable PD, Dann HM, Morin DE and Drackley JK (2009) Liver phosphorus content in Holstein-Friesian cows during the transition period. *J Dairy Sci* **92**:2106-2117.

Guo C, He L, Yao D, A J, Cao B, Ren J, Wang G and Pan G (2014) Alpha-naphthylisothiocyanate modulates hepatobiliary transporters in sandwich-cultured rat hepatocytes. *Toxicol Lett* **224**:93-100.

Hayashi H, Takada T, Suzuki H, Onuki R, Hofmann AF and Sugiyama Y (2005) Transport by vesicles of glycine- and taurine-conjugated bile salts and taurolithocholate 3-sulfate: a comparison of human BSEP with rat Bsep. *Biochim Biophys Acta* **1738**:54-62.

Hirano M, Maeda K, Shitara Y and Sugiyama Y (2006) Drug-drug interaction between pitavastatin and various drugs via OATP1B1. *Drug Metab Dispos* **34**:1229-1236.

Kalvass JC, Maurer TS and Pollack GM (2007) Use of plasma and brain unbound fractions to assess the extent of brain distribution of 34 drugs: comparison of unbound concentration ratios to in vivo p-glycoprotein efflux ratios. *Drug Metab Dispos* **35**:660-666.

Lai Yr (2014) Transporters in Drug Discovery and Development: Detailed Concepts and Best Practice. Woodhead Publishing.

Lee JK, Marion TL, Abe K, Lim C, Pollock GM and Brouwer KLR (2010) Hepatobiliary disposition of troglitazone and metabolites in rat and human sandwich-cultured hepatocytes: use of Monte Carlo simulations to assess the impact of changes in biliary excretion on troglitazone sulfate accumulation. *J Pharmacol Exp Ther* **332**:26-34.

Lepist EI, Gillies H, Smith W, Hao J, Hubert C, St Claire RL, 3rd, Brouwer KR and Ray AS (2014) Evaluation of the endothelin receptor antagonists ambrisentan, bosentan, macitentan, and sitaxsentan as hepatobiliary transporter inhibitors and substrates in sandwich-cultured human hepatocytes. *PloS One* **9**:e87548.

Leslie EM, Watkins PB, Kim RB and Brouwer KLR (2007) Differential inhibition of rat and human Na+-dependent taurocholate cotransporting polypeptide (NTCP/SLC10A1)by bosentan: a mechanism for species differences in hepatotoxicity. *J Pharmacol Exp Ther* 321:1170-1178.

Mateus A, Matsson P and Artursson P (2013) Rapid measurement of intracellular unbound drug concentrations. *Mol Pharm* **10**:2467-2478.

Matsunaga N, Kaneko N, Staub AY, Nakanishi T, Nunoya KI, Imawaka H and Tamai I (2016) Analysis of metabolic pathway of bosentan and cytotoxicity of bosentan metabolites based on a quantitative modeling of metabolism and transport in sandwich-cultured human hepatocytes. *Drug Metab Dispos* **44**:16-27.

Matsunaga N, Wada S, Nakanishi T, Ikenaga M, Ogawa M and Tamai I (2014) Mathematical modeling of the in vitro hepatic disposition of mycophenolic acid and its glucuronide in sandwich-cultured human hepatocytes. *Mol Pharm* **11**:568-579.

Mita S, Suzuki H, Akita H, Hayashi H, Onuki R, Hofmann AF and Sugiyama Y (2006) Vectorial transport of unconjugated and conjugated bile salts by monolayers of LLC-PK1 cells doubly transfected with human NTCP and BSEP or with rat Ntcp and Bsep. *Am J Physiol Gastrointest Liver Physiol* **290**:G550-556.

Morgan RE, Trauner M, van Staden CJ, Lee PH, Ramachandran B, Eschenberg M, Afshari CA, Qualls CW, Jr., Lightfoot-Dunn R and Hamadeh HK (2010) Interference with bile salt export pump function is a susceptibility factor for human liver injury in drug development. *Toxicol Sci* **118**:485-500.

Morgan RE, van Staden CJ, Chen Y, Kalyanaraman N, Kalanzi J, Dunn RT, 2nd, Afshari CA and Hamadeh HK (2013) A multifactorial approach to hepatobiliary transporter assessment enables improved therapeutic compound development. *Toxicol Sci* **136**:216-241.

Noe J, Stieger B and Meier PJ (2002) Functional expression of the canalicular bile salt export pump of human liver. *Gastroenterology* **123**:1659-1666.

Nozawa T, Imai K, Nezu J, Tsuji A and Tamai I (2004) Functional characterization of pH-sensitive organic anion transporting polypeptide OATP-B in human. *J Pharmacol Exp Ther* **308**:438-445.

Oshio C and Phillips MJ (1981) Contractility of bile canaliculi: implications for liver function. *Science (New York, NY)* **212**:1041-1042.

Pfeifer ND, Goss SL, Swift B, Ghibellini G, Ivanovic M, Heizer WD, Gangarosa LM and Brouwer KLR (2013a) Effect of Ritonavir on (99m)Technetium-Mebrofenin Disposition in Humans: A Semi-PBPK Modeling and In Vitro Approach to Predict Transporter-Mediated DDIs. *CPT Pharmacometrics Syst Pharmacol* **2**:e20.

Pfeifer ND, Harris KB, Yan GZ and Brouwer KLR (2013b) Determination of intracellular unbound concentrations and subcellular localization of drugs in rat sandwich-cultured hepatocytes compared with liver tissue. *Drug Metab Dispos* **41**:1949-1956.

Pfeifer ND, Yang K and Brouwer KLR (2013c) Hepatic basolateral efflux contributes significantly to rosuvastatin disposition I: characterization of basolateral versus biliary clearance using a novel protocol in sandwich-cultured hepatocytes. *J Pharmacol Exp Ther* **347**:727-736.

Phillips MJ, Oshio C, Miyairi M, Katz H and Smith CR (1982) A study of bile canalicular contractions in isolated hepatocytes. *Hepatology* **2**:763-768.

Rius M, Hummel-Eisenbeiss J, Hofmann AF and Keppler D (2006) Substrate specificity of human ABCC4 (MRP4)-mediated cotransport of bile acids and reduced glutathione. *Am J Physiol Gastrointest Liver Physiol* **290**:G640-649.

Sato M, Iwanaga T, Mamada H, Ogihara T, Yabuuchi H, Maeda T and Tamai I (2008) Involvement of uric acid transporters in alteration of serum uric acid level by angiotensin II receptor blockers. *Pharm Res* **25**:639-646.

Shitara Y, Li AP, Kato Y, Lu C, Ito K, Itoh T and Sugiyama Y (2003) Function of uptake transporters for taurocholate and estradiol 17beta-D-glucuronide in cryopreserved human hepatocytes. *Drug Metab Pharmacokinet* **18**:33-41.

Smith DA, Di L and Kerns EH (2010) The effect of plasma protein binding on in vivo efficacy: misconceptions in drug discovery. *Nat Rev Drug Discov* **9**:929-939.

Sohlenius-Sternbeck AK (2006) Determination of the hepatocellularity number for human, dog, rabbit, rat and mouse livers from protein concentration measurements. *Toxicol In Vitro* **20**:1582-1586.

Swift B, Pfeifer ND and Brouwer KLR (2010) Sandwich-cultured hepatocytes: an in vitro model to evaluate hepatobiliary transporter-based drug interactions and hepatotoxicity. *Drug Metab Rev* **42**:446-471.

Vildhede A, Mateus A, Khan EK, Lai Y, Karlgren M, Artursson P and Kjellsson MC (2016) Mechanistic Modeling of Pitavastatin Disposition in Sandwich-Cultured Human Hepatocytes: A Proteomics-Informed Bottom-Up Approach. *Drug Metab Dispos* **44**:505-516.

Vildhede A, Wisniewski JR, Noren A, Karlgren M and Artursson P (2015) Comparative Proteomic Analysis of Human Liver Tissue and Isolated Hepatocytes with a Focus on Proteins Determining Drug Exposure. *J Proteome Res* **14**:3305-3314.

Weber C, Gasser R and Hopfgartner G (1999) Absorption, excretion, and metabolism of the endothelin receptor antagonist bosentan in healthy male subjects. *Drug Metab Dispos* **27**:810-815.

Wisniewski JR, Vildhede A, Noren A and Artursson P (2016) In-depth quantitative analysis and comparison of the human hepatocyte and hepatoma cell line HepG2 proteomes. *J Proteomics* **16**:136:234-47.

Wolf KK, Brouwer KR, Pollack GM and Brouwer KLR (2008) Effect of albumin on the biliary clearance of compounds in sandwich-cultured rat hepatocytes. *Drug Metab Dispos* **36**:2086-2092.

Woodhead JL, Yang K, Siler SQ, Watkins PB, Brouwer KLR, Barton HA and Howell BA (2014) Exploring BSEP inhibition-mediated toxicity with a mechanistic model of drug-induced liver injury. *Front Pharmacol* **5**: 240.

Yang K, Guo C, Woodhead JL, St Claire RL, 3rd, Watkins PB, Siler SQ, Howell BA and Brouwer KLR (2016) Sandwich-Cultured Hepatocytes as a Tool to Study Drug Disposition and Drug-Induced Liver Injury. *J pharm sci* **105**:443-459.

Yang K, Pfeifer ND, Kock K and Brouwer KLR (2015) Species Differences in Hepatobiliary Disposition of Taurocholic Acid in Human and Rat Sandwich-Cultured Hepatocytes: Implications for Drug-Induced Liver Injury. *J Pharmacol Exp Ther* **353**:415-23.

Yang K, Woodhead JL, Watkins PB, Howell BA and Brouwer KLR (2014) Systems pharmacology modeling predicts delayed presentation and species differences in bile acid-mediated troglitazone hepatotoxicity. *Clin Pharmacol Ther* **96**:589-598.

Zhang DW, Gu HM, Vasa M, Muredda M, Cole SP and Deeley RG (2003) Characterization of the role of polar amino acid residues within predicted transmembrane helix 17 in determining the substrate specificity of multidrug resistance protein 3. *Biochemistry* **42**:9989-10000.

Zuber C, Spiro MJ, Guhl B, Spiro RG and Roth J (2000) Golgi apparatus immunolocalization of endomannosidase suggests post-endoplasmic reticulum glucose trimming: implications for quality control. *Mol Biol Cell* **11**:4227-4240.

Footnote

This research was supported by the National Institute of General Medical Sciences of the National Institutes of Health [R01GM041935]. The content is solely the responsibility of the authors and does not necessarily represent the official views of the NIH. Cen Guo is supported, in part, by the UNC Royster Society of Fellows.

B-CLEAR® is covered by US Pat. No. 6,780,580 and other US and International patents both issued and pending.

This work was presented, in part, as a poster at the 19th North American International Society for the Study of Xenobiotics (ISSX) Meeting/29th Japanese Society for the Study of Xenobiotics (JSSX) Meeting (2014): Guo, C., Brouwer, K.R., Yang, K., St. Claire, R. and Brouwer, K.L.R. Prediction of altered bile acid disposition by drugs using an integrated approach: Sandwich-cultured human hepatocytes, mechanistic modeling and simulation. This work was presented, in part, as a poster and podium presentation at the 20th North American International Society for the Study of Xenobiotics (ISSX) Meeting (2015): Guo, C., Yang, K., and Brouwer, K.L.R. Prediction of hepatic efflux transporter-mediated DDIs: when does variability in IC_{50} or intracellular unbound fraction of inhibitors matter?

Figure Legends

Fig. 1. (A) Model schemes depicting disposition of d_8-TCA in sandwich-cultured human hepatocytes (SCHH) using standard (Cells+Bile) Hanks' balanced salt solution (HBSS) (left) and Ca^{2+}-free (Cells) HBSS (right). (B) d_8-TCA mass vs. time data in SCHH lysate (left) and incubation buffer (right). Closed symbols/solid lines represent d_8-TCA in Cells + Bile or standard HBSS, and open symbols/dashed lines represent d_8-TCA in Cells or Ca^{2+}-free HBSS. Experimental data (circles) represent the mean ± S.E.M. (n = 3 SCHH preparations in triplicate per group). The simulated profiles (lines) were generated from Equations 1-5 using the mean of best-fit parameter estimates from 3 SCHH datasets (Table 2).

Fig. 2. Impact of impaired CL_{Uptake} and CL_{Efflux} (CL_{Efflux}= CL_{BL}+ CL_{Bile}) of TCA on different model outputs: (A) TCA total concentration in Cells ($C_{t,Cells}$), (B) TCA total amount in Cells+Bile ($X_{t,Cells+Bile}$), (C) TCA total amount in Bile ($X_{t,Bile}$), (D) Ratio of the total amount of TCA in Cells to the total amount of TCA in Cells+Bile ($X_{t,Cells}/X_{t,Cells+Bile}$), (E) Ratio of the total amount of TCA in Bile to the total amount of TCA in Cells ($X_{t,Bile}/X_{t,Cells}$), and (F) Ratio of the total amount of TCA in Bile to the total amount of TCA in Cells+Bile ($X_{t,Bile}/X_{t,Cells+Bile}$) in SCHH. The Z-axis represents the fold change compared to baseline (shown in the color map on the right), based on simulations of TCA accumulation at steady state. Figures C, E, and F have been rotated to improve visibility of the 3-D surface.

Fig. 3. Sensitivity analysis of cellular unbound fraction of inhibitor ($f_{u,cell,inhibitor}$) for telmisartan and bosentan. Fold changes in the TCA $C_{t,Cells}$ at steady state compared to baseline (without inhibitors), in the presence of telmisartan and bosentan were simulated based on the average IC_{50} values (Table 1), cellular total inhibitor concentration (Table 3), and different $f_{u,cell,inhibitor}$ values using a Monte Carlo simulation approach. Data were expressed as mean and S.D. of 40 simulated individuals.

Fig. 4. The sensitivity of the predicted TCA $C_{t,Cells}$ to changes in $f_{u,cell,inhibitor}$ as a function of ($[I]_{t,cell}/IC_{50}$) values for a set of theoretical inhibitors. TCA $C_{t,Cells}$ in the presence of theoretical inhibitors with different ($[I]_{t,cell}/IC_{50}$) values were simulated assuming $f_{u,cell,inhibitor}$ =1 (black bar) and $f_{u,cell,inhibitor}$ =0.02 (white bar). The fold changes of TCA $C_{t,Cells}$ with inhibitors compared to without inhibitors are plotted on the y-axis.

JPET Fast Forward. Published on May 27, 2016 as DOI: 10.1124/jpet.116.231928
This article has not been copyedited and formatted. The final version may differ from this version.

Fig. 5. Proposed framework to predict altered bile acid disposition in sandwich-cultured human hepatocytes (SCHH) mediated by inhibition of multiple transporters. Black solid boxes represent experimental observations, and black double-lines depict the simulation output, as detailed in the Discussion. The kinetic parameters, including uptake clearance (CL_{Uptake}), biliary clearance (CL_{Bile}), and basolateral efflux clearance (CL_{BL}), of the victim bile acid (e.g. taurocholic acid) are estimated by using mechanistic modeling; in the presence of inhibitors, the clearance values ($CL_{inhibitor}$) are estimated using Equations 7-10 based on inhibitor concentrations in the medium or cells ($[I]_{cell}$) and IC_{50} or K_i values. The choice of which $[I]_{cell}$ to use depends on the ($[I]_{t,cell}/IC_{50}$) value of the inhibitor, where $[I]_{t,cell}$ represents cellular total concentration of inhibitor. If this value is high, the cellular unbound fraction of inhibitor ($f_{u,cell,inhibitor}$) should be measured to estimate $[I]_{u,cell}$, where $[I]_{u,cell}$ represents the cellular unbound concentration of inhibitor. Otherwise, $[I]_{t,cell}$ can be used. Finally, the altered cellular total concentrations ($C_{t,Cells}$) of the victim bile acid are simulated using $CL_{inhibitor}$.

JPET Fast Forward. Published on May 27, 2016 as DOI: 10.1124/jpet.116.231928
This article has not been copyedited and formatted. The final version may differ from this version.

Table 1. Inhibition constants (μM) of telmisartan and bosentan against transporters involved in the hepatic uptake and efflux of TCA.

Clearance	**Transporter**	**Telmisartan**	**Reference**	**Bosentan**	**Reference**
CL_{Uptake}	NTCP	60 (K_i)	(Dong et al., 2014)	18 (K_i)	(Leslie et al., 2007)
				36 (IC_{50})	(Lepist et al., 2014)
	OATP1B1	0.44 (K_i)	(Hirano et al., 2006)	18 [a]	
CL_{Bile}	BSEP	16-16.2 (IC_{50})	(Lai, 2014), (Morgan et al., 2013)	23-42 (IC_{50})	(Morgan et al., 2013) (Lepist et al., 2014)
CL_{BL}	MRP4	11-36 (IC_{50})	(Sato et al., 2008) (Morgan et al., 2013)	22 (IC_{50})	Morgan et al., 2013
	MRP3	60 (IC_{50})	(Morgan et al., 2013)	42 (IC_{50})	(Morgan et al., 2013)

[a] *not available and therefore assumed to be the same as NTCP*

JPET Fast Forward. Published on May 27, 2016 as DOI: 10.1124/jpet.116.231928
This article has not been copyedited and formatted. The final version may differ from this version.

Table 2. Recovered estimates of d_8-TCA total uptake clearance (CL_{Uptake}), basolateral efflux clearance (CL_{BL}), biliary clearance (CL_{Bile}) and K_{Flux} in the presence of 4% BSA. Estimates were based on the model scheme and time-course data depicted in Fig.1. The model was fit to data generated from n=3 independent SCHH preparations (triplicate measurements) separately.

Parameter Estimate	**Mean**	**SD**	**CV%**
CL_{Uptake} (*mL/min/g liver*)	0.63	0.12	20
CL_{BL} (*mL/min/g liver*)	0.034	0.011	32
CL_{Bile} (*mL/min/g liver*)	0.074	0.030	36
K_{Flux} (min^{-1})	0.018	0.0015	8

JPET Fast Forward. Published on May 27, 2016 as DOI: 10.1124/jpet.116.231928
This article has not been copyedited and formatted. The final version may differ from this version.

Table 3. Measured total and unbound concentrations of inhibitors ($[I]_t$ and $[I]_u$, μM) in the medium ($[I]_{med}$), whole cell lysate ($[I]_{cell}$), and cytosol ($[I]_{cyt}$). SCHH were treated with telmisartan (1 or 10 μM) and bosentan (0.8 or 8 μM) for 20 min in the presence of 4% BSA. Data were generated from n=1 SCHH preparation. Unbound concentration and f_u data were expressed as mean values obtained from triplicate measurements and values in parentheses represent ranges. Total concentrations were from single measurements.

Inhibitor	Medium			Cell lysate			Cytosol		
	$[I]_{t,med}$	$[I]_{u,med}$	$f_{u,med}$	$[I]_{t,cell}$	$[I]_{u,cell}$	$f_{u,cell,inhibitor}$	$[I]_{t,cyt}$	$[I]_{u,cyt}$	$f_{u,cyt,inhibitor}$
Telmisartan	1	0.012 (0.0098-0.014)	0.012 (0.0098-0.0134)	16	2.1 (1.6-2.5)	0.13 (0.099-0.16)	16	0.85 (0.8-0.9)	0.053 (0.050-0.056)
	10	0.20 (0.18-0.22)	0.02 (0.018-0.022)	40	3.7 (2.7-4.8)	0.094 (0.068-0.12)	35	2.8 (1.8-3.4)	0.080 (0.052-0.098)
Bosentan	0.8	0.031 (0.023-0.039)	0.039 (0.029-0.048)	1.9	0.79 (0.66-0.93)	0.41 (0.34-0.48)	1.7	0.21 (0.21-0.21)	0.12 (0.12-0.12)
	8	0.45 (0.44-0.47)	0.057 (0.055-0.058)	17	3.8 (3.1-4.5)	0.22 (0.18-0.26)	14	N/A[a]	N/A[a]

[a] *N/A: not available*

JPET Fast Forward. Published on May 27, 2016 as DOI: 10.1124/jpet.116.231928
This article has not been copyedited and formatted. The final version may differ from this version.

Table 4. Experimentally observed and simulated alteration of TCA total concentration in Cells ($C_{t,Cells}$) due to telmisartan and bosentan. Observed data are presented as fold change in the presence compared to the absence of inhibitors. SCHH were pre-treated with telmisartan (1 and 10 µM) or bosentan (0.8 and 8 µM) for 10 min, followed by co-incubation with d_8-TCA and telmisartan or bosentan for 10 min. Observed data represented geometric mean (range) measured in n=1 SCHH preparation in duplicate. Monte Carlo simulations for 40 individuals were performed 10 times using parameter estimates and associated variance (Table 2), different inhibitor concentrations (Table 3), and IC_{50} data (Table 1) assuming CL_{Uptake} was mediated by NTCP (70%) and OATPs (30%), CL_{Bile} was mediated by BSEP, and CL_{BL} was governed by MRP3. Simulation data are presented as arithmetic mean of 10 simulations (95% confidence interval). Average fold errors were calculated based on Equation 12.

Inhibitor	Dosing conc.	Fold Change in TCA $C_{t,Cells}$				
		Observation	Simulation			
			$[I]_{t,cell}$	$[I]_{u,cell}$	$[I]_{t,cyt}$	$[I]_{u,cyt}$
Telmisartan	1 µM	0.91 (0.87-0.95)	1.3 (1.3-1.4)	1.0 (0.99-1.1)	1.3 (1.3-1.3)	1.0 (0.94-1.1)
	10 µM	1.1 (1.0-1.1)	1.4 (1.3-1.4)	1.0 (0.98-1.0)	1.3 (1.3-1.3)	0.96 (0.95-0.98)
	Average fold error		1.4	1.0	1.3	0.99
Bosentan	0.8 µM	0.88 (0.83-0.92)	1.0 (0.99-1.0)	0.99 (0.96-1.0)	1.0 (0.99-1.0)	0.99 (0.97-1.0)
	8 µM	0.81 (0.80-0.82)	1.2 (1.2-1.3)	1.0 (1.0-1.1)	1.1 (1.1-1.2)	N/A[a]

	Average fold error	1.3	1.2	1.3	N/A[a]

[a] *N/A: not available*

Fig. 1

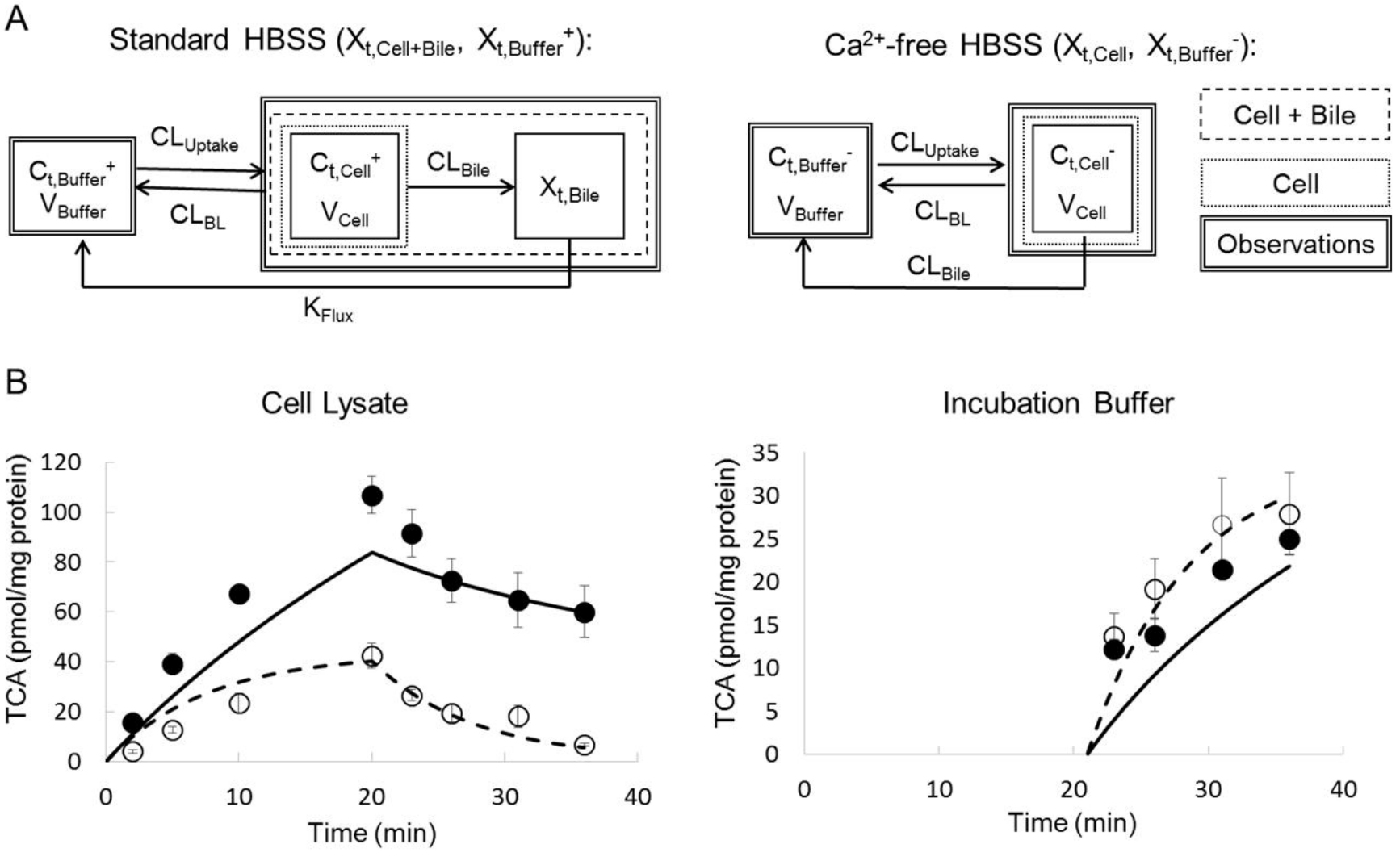
A
Standard HBSS ($X_{t,Cell+Bile}$, $X_{t,Buffer}^{+}$):
$C_{t,Buffer}^{+}$
V_{Buffer}
CL_{Uptake}
CL_{BL}
$C_{t,Cell}^{+}$
V_{Cell}
CL_{Bile}
$X_{t,Bile}$
K_{Flux}
Ca^{2+}-free HBSS ($X_{t,Cell}$, $X_{t,Buffer}^{-}$):
$C_{t,Buffer}^{-}$
V_{Buffer}
CL_{Uptake}
CL_{BL}
$C_{t,Cell}^{-}$
V_{Cell}
CL_{Bile}
Cell + Bile
Cell
Observations
B
Cell Lysate
TCA (pmol/mg protein)
Time (min)
Incubation Buffer
TCA (pmol/mg protein)
Time (min)

Fig. 2

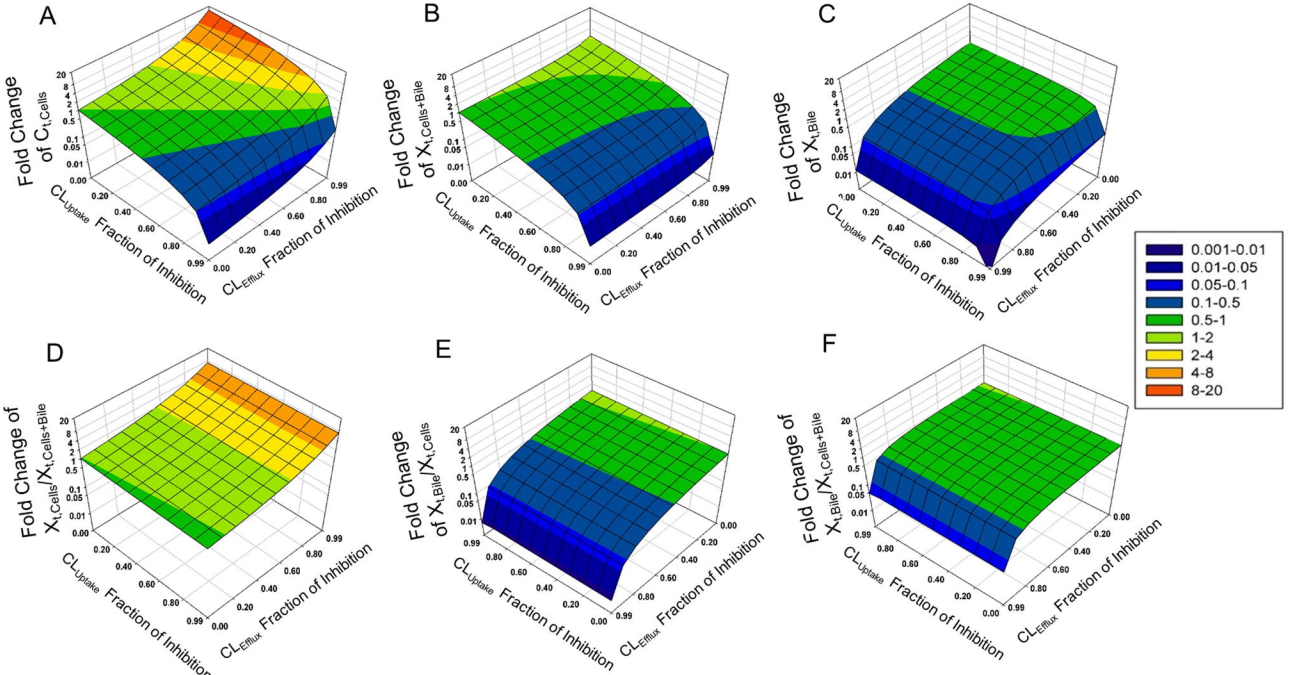
A
Fold Change of $C_{t,Cells}$
B
Fold Change of $X_{t,Cells+Bile}$
C
Fold Change of $X_{t,Bile}$
D
Fold Change of $X_{t,Cells}/X_{t,Cells+Bile}$
E
Fold Change of $X_{t,Bile}/X_{t,Cells}$
F
Fold Change of $X_{t,Bile}/X_{t,Cells+Bile}$
CL_{Uptake} Fraction of Inhibition
CL_{Efflux} Fraction of Inhibition
20
8
4
2
1
0.5
0.1
0.05
0.01
0.00
0.20
0.40
0.60
0.80
0.99
0.001-0.01
0.01-0.05
0.05-0.1
0.1-0.5
0.5-1
1-2
2-4
4-8
8-20

Fig. 3

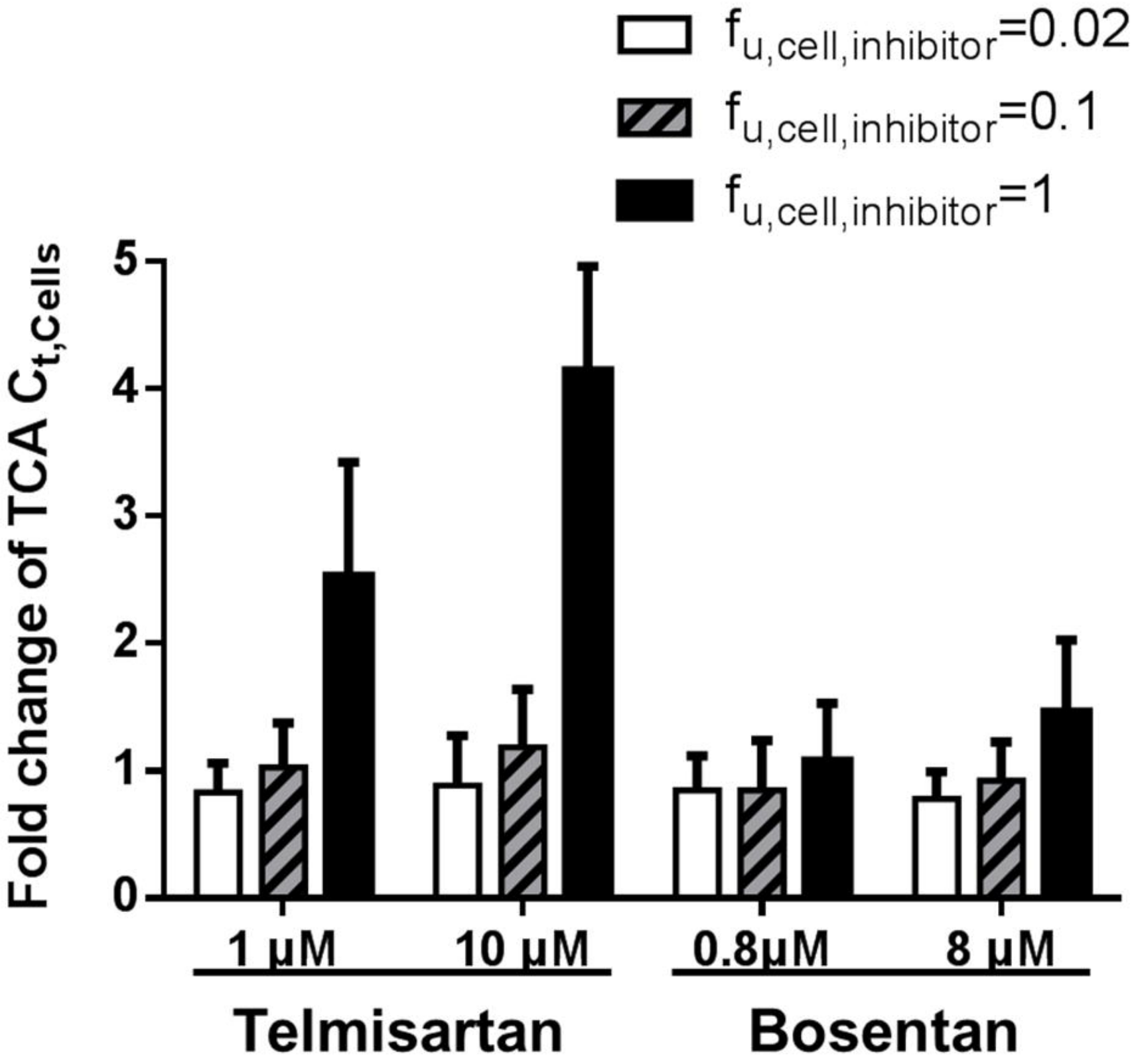
$f_{u,cell,inhibitor}$=0.02
$f_{u,cell,inhibitor}$=0.1
$f_{u,cell,inhibitor}$=1
Fold change of TCA $C_{t,Cells}$
0
1
2
3
4
5
1 µM
10 µM
0.8µM
8 µM
Telmisartan
Bosentan

Fig. 4

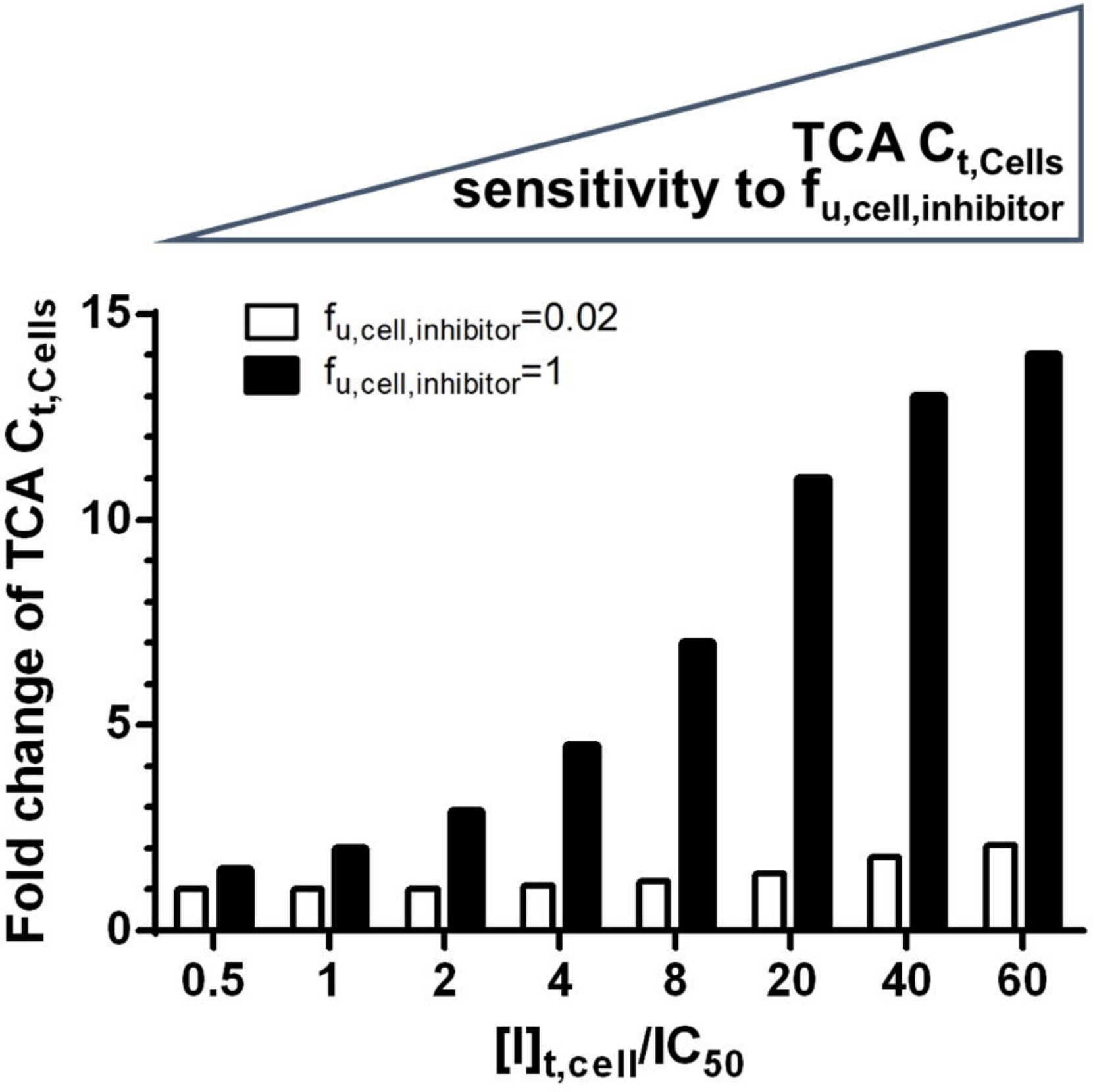
TCA $C_{t,Cells}$ sensitivity to $f_{u,cell,inhibitor}$
$f_{u,cell,inhibitor}$=0.02
$f_{u,cell,inhibitor}$=1
Fold change of TCA $C_{t,Cells}$
0
5
10
15
0.5
1
2
4
8
20
40
60
$[I]_{t,cell}/IC_{50}$

Fig. 5

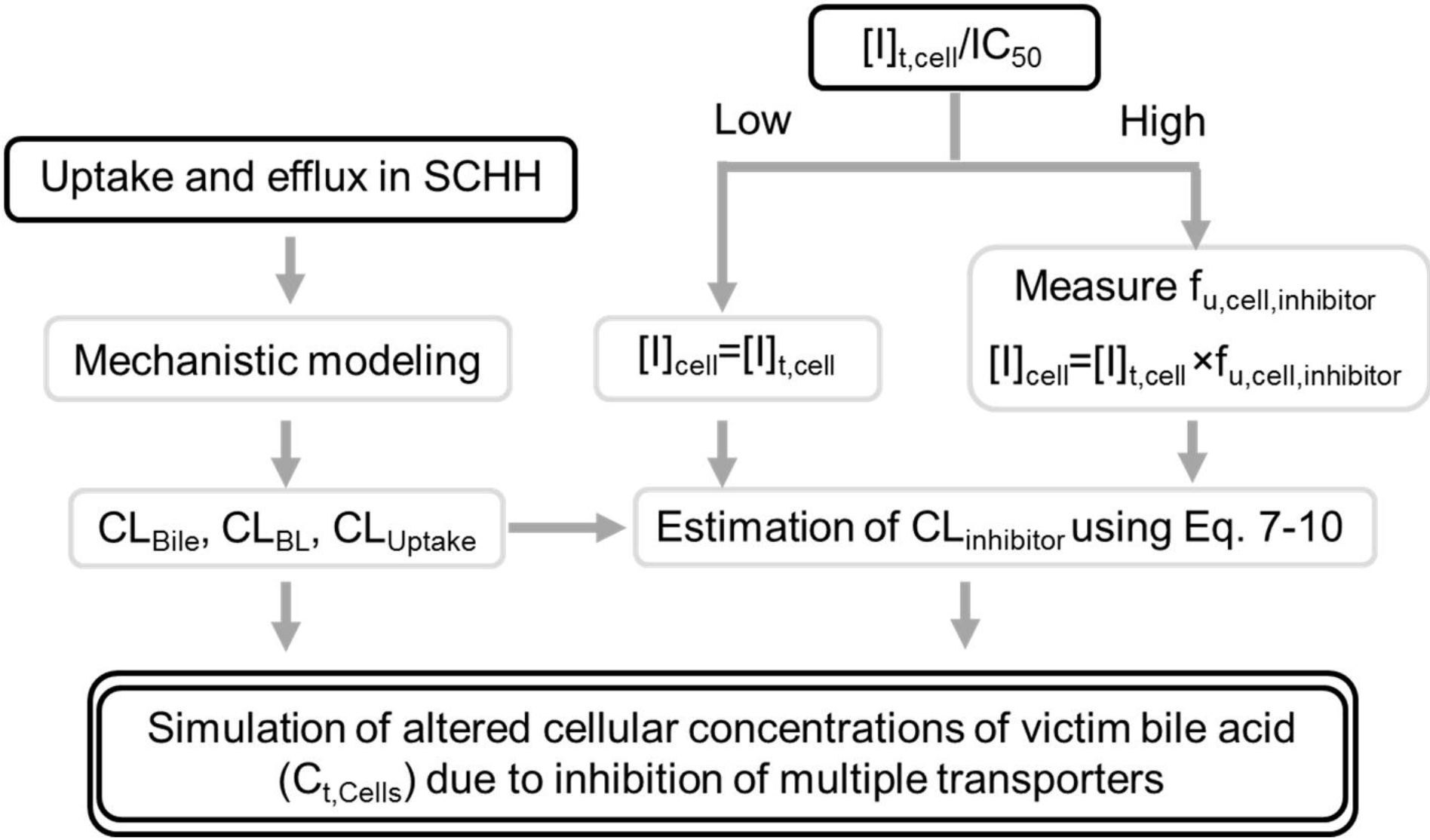
$[I]_{t,cell}/IC_{50}$
Low
High
Uptake and efflux in SCHH
Mechanistic modeling
$[I]_{cell}=[I]_{t,cell}$
Measure $f_{u,cell,inhibitor}$
$[I]_{cell}=[I]_{t,cell} \times f_{u,cell,inhibitor}$
CL_{Bile}, CL_{BL}, CL_{Uptake}
Estimation of $CL_{inhibitor}$ using Eq. 7-10
Simulation of altered cellular concentrations of victim bile acid ($C_{t,Cells}$) due to inhibition of multiple transporters